Submitted to Nuclear Physics B

UCRL-19491
Preprint

c.2

K^--d ELASTIC SCATTERING AND $K^-d \rightarrow K^-pn$ BETWEEN 810 AND 1110 MeV/c

RECEIVED
LAWRENCE
RADIATION LABORATORY
APR 15 1970
LIBRARY AND
DOCUMENTS SECTION

N. N. Jew and G. E. Kalmus

February 1970

AEC Contract No. W-7405-eng-48

TWO-WEEK LOAN COPY

This is a Library Circulating Copy which may be borrowed for two weeks. For a personal retention copy, call Tech. Info. Division, Ext. 5545

LAWRENCE RADIATION LABORATORY
UNIVERSITY of CALIFORNIA BERKELEY

UCRL-19491

DISCLAIMER

This document was prepared as an account of work sponsored by the United States Government. While this document is believed to contain correct information, neither the United States Government nor any agency thereof, nor the Regents of the University of California, nor any of their employees, makes any warranty, express or implied, or assumes any legal responsibility for the accuracy, completeness, or usefulness of any information, apparatus, product, or process disclosed, or represents that its use would not infringe privately owned rights. Reference herein to any specific commercial product, process, or service by its trade name, trademark, manufacturer, or otherwise, does not necessarily constitute or imply its endorsement, recommendation, or favoring by the United States Government or any agency thereof, or the Regents of the University of California. The views and opinions of authors expressed herein do not necessarily state or reflect those of the United States Government or any agency thereof or the Regents of the University of California.

K^--d Elastic Scattering and $K^-d \rightarrow K^-pn$ Between 810 and 1110 MeV/c

N. N. Jew and G. E. Kalmus

Lawrence Radiation Laboratory
University of California
Berkeley, California 94720

February 1970

ABSTRACT

We present here angular distributions for the reactions $Kd \rightarrow Kd$ and $Kd \rightarrow Kpn$ at incident K^- momenta of 810, 910, 1010, and 1110 MeV/c. Data are also presented on K^-n elastic scattering assuming the impulse approximation is valid.

This experiment was done with a two-stage separated K^- beam[1], using as detector the Lawrence Radiation Laboratory 25-inch bubble chamber filled with deuterium.

A total of 219 000 pictures was taken at incident K^- momenta of 810 MeV/c (23 000 pictures), 910 MeV/c (76 000 pictures), 1010 MeV/c (54 000 pictures), and 1110 MeV/c (66 000 pictures). We scanned for two-prong events which had a positive track of projected length $\geq$ 1 mm. About 1/2 the film (80%, 33%, 72%, 49%, respectively, for the four incident momenta) was scanned with just this cut. The remaining half was scanned with the additional restriction that the positive track be of projected length $\leq$ 9 cm and hence must stop within the bubble chamber.

This latter part was used only for the K^-d elastic part of the experiment. The first half was used for both the K^-d elastic and the breakup reactions. The fiducial volume was such that apart from very steep tracks, the origins were more than 9 cm (projected on the scan table) from the chamber boundaries. The number of events found in the portion of the film scanned with no upper limit on the positive track length was about 2.3 times that of the other half. The lower cut was imposed to avoid picking up counterfeit events, the short prong of which was really a low-energy δ ray. In K^--deuteron elastic scattering, this cut limits our angular distributions to regions away from the forward direction $-t \geq 0.02\ (\mathrm{GeV/c})^2$. It presents no difficulties in our analysis of the elastic scattering data. However, for the reaction in which the deuteron is broken up into a free proton and a free neutron, corrections must be put in

to account for this cut. This point required a modification of the theoretical formula we used in our analysis of the data. This analysis is presented in detail in Ref. 2.

Due to the large number of events in the film containing a Σ and one other prong, and also due to the difficulty of measuring the momenta of short tracks from curvature, we rejected all events which had a scatter or kink occurring in the first 4 cm (projected) of the outgoing tracks. From the known pd, dd, and K^-d total cross sections, we estimate that this criterion rejected 4±2% of the genuine events in the breakup reaction and 3±2% in the K^-d elastic reaction.

Any event with a V pointing at the origin of the two-prong interaction was rejected at the time of scanning. In cases of ambiguous origins, the event was accepted for measuring and fitting.

The scanning yielded a total of 44 000 two-prong events. These were then measured on the Franckenstein measuring system. About half of these events were measured before these measuring machines went under automatic computer control. The remaining half was measured with these machines under computer control provided by the COBWEB system[3]. The momenta of all stopping tracks were obtained from range measurements. Events that failed at either the measuring stage or the spatial reconstruction stage were remeasured. We estimate that less than 1% of the scanned events were missing after the remeasurements.

The measured events were processed through the FOG-CLOUDY-FAIR system of geometry reconstruction, kinematic fitting, and data selection computer programs.

Of the 44 000 two-prong events that came through the system of fitting programs, the breakdown into the number of events fitting the three interaction hypotheses

$$K^-d \rightarrow K^-d \qquad \text{(H1)}$$
$$\rightarrow K^-pn \qquad \text{(H2)}$$
$$\rightarrow K^-p\Lambda \ (\Lambda \text{ not seen}) \qquad \text{(H3)}$$

are displayed in Venn diagrams in Fig. 1. The criteria we used for these selections were the χ^2 for each fit:

$$\chi^2(K^-d) \leq 10 \quad , \quad \text{four-constraint fit,}$$
$$\chi^2(K^-pn) \leq 4 \quad , \quad \text{one-constraint fit,}$$
$$\chi^2(\pi^-p\Lambda) \leq 4 \quad , \quad \text{one-constraint fit.}$$

These cutoff values for the χ^2 are the limits within which approximately 95% of the area under the theoretical χ^2 distributions are included.

As can be seen from the diagrams in Fig. 1, a majority of the events (≈86% for the four momenta together) fitting the elastic scattering hypothesis also fit the K^-pn hypothesis. This is not an unexpected result, since the deuteron can simulate the breakup reaction, with the neutron and the proton seen as going off in the same direction. When a deuteron is mistaken for a proton, or vice versa, range measurements give values for the momentum of the track that differ from the actual momentum by 60 to 100 MeV/c. But a one-constraint fitting hypothesis would not be able to distinguish this difference in the majority of cases. This is reflected in good χ^2 values for both hypotheses. The ionization is not of help in the identification either.

Both the proton and the deuteron appear as solid, dark tracks in the range of momentum values with which they emerge from the interaction with the incident K^- particle. However, the elastic scattering reaction is a four-constraint fitting hypothesis, whereas the breakup reaction has only one constraint. To get a sample of elastic events, we made the assumption that all the events fitting the elastic reaction are good K^-d elastic scattering events. In order to include as few breakup events as possible in this sample, we made use of an additional handle. As noted above, the deuteron can simulate the breakup reaction, but only with the proton and neutron seen going off in nearly the same direction. This means that the angle between the proton and the neutron tracks, when the events are put through the breakup hypothesis, should be around 0 deg for genuine elastic scattering events. The real breakup events should have a uniform distribution in this angle, since in this case the neutron and the proton are not strongly correlated. In Fig. 2 we have plotted the distribution of events as a function of the cosine of the angle between the proton and the neutron for the K^-pn hypothesis when applied to the K^-d elastic scattering events. We note that almost all the events ($\approx$84%) fall within the interval between 0.9 and 1.0. As our final sample of K^-d elastic scattering events we took only the events in the interval between 0.5 and 1.0 in cos (n-p). These were subsequently corrected for biases and losses (to be considered below).

As our sample of breakup events, we took all the events that satisfied hypothesis H2 (as determined by the χ^2) and subtracted

those that also fitted the K^-d elastic-scattering criteria described above. In Fig. 3, we have plotted the histograms of the cosine of the angle between the proton and the neutron for these events. The excess of events in the forward boxes represents K^-d elastic-scattering events which have $\chi^2 > 10$ for hypothesis H1. These large χ^2 events occur at small momentum transfers in the breakup distributions. We removed this contamination to the breakup events by using only the part of the breakup distribution above $-t = 0.06$ $(GeV/c)^2$ in our analysis. The corrections due to excluding these large χ^2 events from the K^-d elastic distributions are considered below. We have included in our sample of $K^-d \rightarrow K^-pn$ events only those from film scanned with no upper limit on the length of the outgoing proton track.

From the diagrams in Fig. 1, we see that a large number ($\approx$40%) of the K^-d elastic scattering events fit also the $\pi^-p\Lambda$ hypothesis H3. To determine what fraction of this number represents actual $\pi^-p\Lambda$ events, we examine Fig. 4. This is a missing-mass histogram resulting from having all the events that satisfied hypothesis H1 treated as hypothesis H3. We see that for each momentum the mass peak is less than the Λ rest mass. This is consistent with misidentifying the K^-d elastic scattering events as $\pi^-p\Lambda$ events. From the absence of a bump near the Λ rest mass, we estimate that the Λ contamination was negligible (less than 1%) in our sample of K^-d elastic scattering events.

For the breakup reaction, we estimated the contamination from the $\pi^-p\Lambda$ events in another way. It was found in Ref. 4 that there should be 1350 $\pi^-p\Lambda$ events and 480 $\pi^-p\Sigma^\circ$ events in the 1.11 GeV/c

film that had a spectator proton track between 1.5 mm and 6 cm in length. The two numbers include both the visible and invisible decay modes of the Λ. They also include corrections to bring their cross sections into agreement with other experiments considered in Ref. 4. From a separate scan, we also found that there were 590 events fitting $\pi^- p\Lambda$ and 530 fitting $\pi^- p\Sigma^\circ$, with the spectator proton track longer than 6 cm. Combining these numbers gives 2950 events with a Λ in the final state. Only 1/3 of these Λ's ($\approx$980) decay via the invisible mode $n\pi^\circ$. Since we used only half the film at 1.11 GeV/c for the breakup reaction, we have included only half this number of Λ's ($\approx$490) in our sample. From the fit of our sample to hypothesis H3, we have 526 events that fitted only this hypothesis. Thus we see that the $\pi^- p\Lambda$ events are separated by the χ^2 selection. We conclude that the Λ contamination is also small in the breakup reaction (less than 2%) of the 1.11 GeV/c sample. We have not scanned for $\pi^- p\Lambda$ events with long spectator proton tracks for the remaining three momenta. But from the number of events fitting only hypothesis H3 in these momenta, we estimate the Λ contamination to be about the same as in the 1.11 GeV/c sample.

In scanning for events for this experiment, we had imposed the criterion that each event must have a positive track longer than 1 mm. This cut was imposed for measuring purposes. Unfortunately, this introduced a bias against events with a short positive track pointing along the camera axis, which was up-and-down with respect to the bubble chamber. (The beam entered the chamber in a horizontal plane

at mid-chamber. The three cameras were positioned at the bottom, looking vertically up.) These events appeared foreshortened on film. Figures 5 and 6, showing the distribution of events as a function of the azimuthal angle of the positive track about the beam axis, clearly illustrate this scanning bias. If there were no biases, these distributions would be uniform. The bias causes a depletion of events in the forward direction in the angular distributions, thus effectively flattening their slope. To avoid this effect, we have included in our distributions only those events with the positive track coming out of the interaction vertex within 45 deg of the horizontal plane. The only exception to this is the distribution for the breakup reaction at 0.81 GeV/c. Since we do not have many events at this incident momentum and since the azimuthal angular distribution for the breakup reaction at this momentum does not show a serious bias, we have included all the events at this momentum.

The experimental χ^2 distributions for the K^-d elastic scattering hypothesis at the four incident momenta are shown in Fig. 7. As is quite common, these experimental distributions have a large tail. One way to correct for this long-tail effect is to accept events up to $\chi^2 = 20$ as K^-d elastic scattering events. We have decided to accept events up to $\chi^2 = 10$, which is normal for χ^2 of four degrees of freedom. We account for the events in the tail by correcting the number of events thus obtained by the excess of events in the experimental tail over those in the theoretical tail (defined by the interval $10 \leq \chi^2 \leq 20$). The correction factor at each incident momentum is shown in Table I, together with other normalization and correction

factors.

Figures 8 and 9 show the t distributions for the reactions $K^-d \rightarrow K^-d$ and $K^-d \rightarrow K^-pn$. The breakup reaction data were obtained with a lower cutoff on the proton momentum of 95 MeV/c at 810, 1010, and 1110 MeV/c, whereas a cut of 130 MeV/c was applied at 910 MeV/c.

The smooth curves are the results of a simultaneous fit to the elastic scattering and the breakup reaction. This analysis of the data is described in detail in Ref. 2. Briefly, it consists of using a modified form of the Glauber formalism[5], which relates the K^-d elastic and the K^-pn (breakup) amplitudes in terms of the K^-p and K^-n elastic scattering amplitudes, including the effect of double scattering. We modified this to include the effect of spin, the difference in the flux factors for K^- incident on a deuteron and on a nucleon, the effect of Fermi-momentum smearing of the nucleon cross sections[6], and the corrections arising from the proton momentum cut made in scanning.

For the fits we need to know the K^-p and K^-n amplitudes. For the K^-p amplitude, we assumed two models based on experimental data in this momentum region[7,8]. The K^-n elastic amplitude was parameterized as a sum of $Y_1^*(1660)$ and $Y_1^*(1765)$ and an exponential background. (We have also tried an s- and a p-wave background.) The only parameters that were allowed to vary in fitting the K^-d and K^-pn data were those of the background amplitude.

It can be seen that the fits to the K^-d elastic scattering cross section (Fig. 8) are good, whereas those to the breakup reaction (Fig. 9) are not very good, especially at large momentum transfer

squared. This is because in this t region there were essentially no free parameters in our models to optimize our fit, so that small inaccuracies in the models had large effects.

In Fig. 10 we show the K^-n elastic cross sections obtained from a simple impulse-approximation method. In obtaining these from the breakup reaction, it was assumed that the interaction was on the neutron if the proton momentum was less than 250 MeV/c and the neutron momentum was greater than 250 MeV/c. The curves are the predictions from the models described above. As a comparison we show in Fig. 11 the K^-p elastic scattering data obtained from our data, now using the impulse approximation with $P_n < 250$ MeV/c and $P_p > 250$ MeV/c. The curves are fits from the published K^-p elastic scattering data[7,8].

We thank Dr. Robert Poe for many helpful discussions; also, all the scanners and measurers of the Powell-Birge group for their meticulous work.

Table I. Normalization and correction factors.

	Beam Momentum (MeV/c)			
	810	910	1010	1110
Number of incident K^-:				
in K^-d (x 10^5)	1.55	6.76	5.04	6.42
in K^-pn (x 10^5)	1.10	2.21	3.63	3.20
π-μ Contamination (%)	4.9	6.0	5.3	9.1
Fiducial Volume Length (cm) (corrected for beam attenuation)	28.8	28.6	28.5	28.7
K^-d χ^2 correction factor	1.12	1.17	1.18	1.13
Scan efficiency (%)				
for K^-d	97.9	96.8	97.3	96.5
for K^-pn	91.7	92.8	92.4	89.6

References

1) R. B. Bell et al., A Variable-Momentum Separated $K^{\pm}$ Beam at the Bevatron, UCRL-11527, July 1964, unpublished

2) N. N. Jew, K^--Neutron Elastic Scattering From $K^-d \rightarrow K^-d$ and $K^-d \rightarrow Kpn$ at 1 BeV/c (Ph.D. thesis), UCRL-19359, Oct. 1969, unpublished

3) H. C. Albrecht et al., The COBWEB Data Reduction System, UCRL-18528(Rev.), Oct. 1968, unpublished

4) W. M. Smart, Study of the Y_1^* Resonant Amplitudes Between 1660 and 1900 MeV in the Reaction $K^-n \rightarrow \Lambda\pi^-$ (Ph.D. thesis), UCRL-17712, Aug. 1967, unpublished

5) R. J. Glauber, in Lectures in Theoretical Physics, edited by W. E. Britten et al. (Interscience Publishers, Inc., New York, 1959), Vol. I, p. 315

6) G. Fäldt and T. E. O. Ericson, Nucl. Phys. B8 (1968) 1

7) T. Lasinski, R. Levi-Setti, and E. Predazzi, Phys. Rev. 163 (1967) 1792

8) R. Armenteros, P. Baillon, C. Breiman, M. Ferro-Luzzi, D. E. Plane, N. Schmitz, E. Burkhardt, H. Filthuth, E. Kluge, H. Oberlack, R. R. Ross, R. Barloutaud, P. Granet, J. Meyer, J. P. Porter, and J. Prevost, Nucl. Phys. B8 (1968) 195

Figure Captions

1. Breakdown of the number of events fitting the different hypotheses. These numbers were obtained from all the film.

2. Distributions in the cosine of the angle between the proton and the neutron resulting from applying the $K^-d \rightarrow K^-pn$ hypothesis to the events fitting K^-d elastic scattering.

3. Distributions in the cosine of the angle between the proton and the neutron for $K^-d \rightarrow K^-pn$ events. The events near cos (p-n) = 1 are due to K^-d elastic events in the tail of the χ^2 distribution.

4. Missing-mass distributions resulting from applying the $K^-d \rightarrow \pi^-p\Lambda$ hypothesis to the $K^-d \rightarrow K^-d$ events.

5. Distributions of the azimuthal angle of the positive track about the beam axis for the $K^-d \rightarrow K^-d$ events.

6. Distributions of the azimuthal angle of the positive track about the beam axis for the $K^-d \rightarrow K^-pn$ events.

7. χ^2 distributions for the $K^-d \rightarrow K^-d$ hypothesis.

8. $K^-d \rightarrow K^-d$ distributions in -t, the K^- momentum transfer squared. The smooth curves are simultaneous fits to our K^-d elastic and breakup reaction data using the Glauber formalism.

9. $K^-d \rightarrow K^-pn$ distribution in -t, the K^- momentum transfer squared. The dashed curves were obtained from our simultaneous fits with an exponential K^-n background amplitude. The solid curves resulted from fits with s and p waves in the K^-n background amplitude.

10. $K^-n \rightarrow K^-n$ differential cross sections. The data points are from impulse approximation K^-n elastic scattering events. Solid curves are from our simultaneous fits with an exponential background in the K^-n amplitude; the dashed curves are from fits with an s and p wave background. The normalization of the data points is relative to the solid curve in the range $-1 < \cos(Kn) < 0.6$.

11. $K^-p \rightarrow K^-p$ differential cross sections. The data points are K^-p impulse approximation distributions from the breakup reaction of our experiment. The solid curves are calculated from the K^-p model of Ref. 7; the dashed curves are calculated from the K^-p model of Ref. 8. The normalization of the data points is relative to the solid curve in the range $-1 < \cos(Kp) < 0.6$.

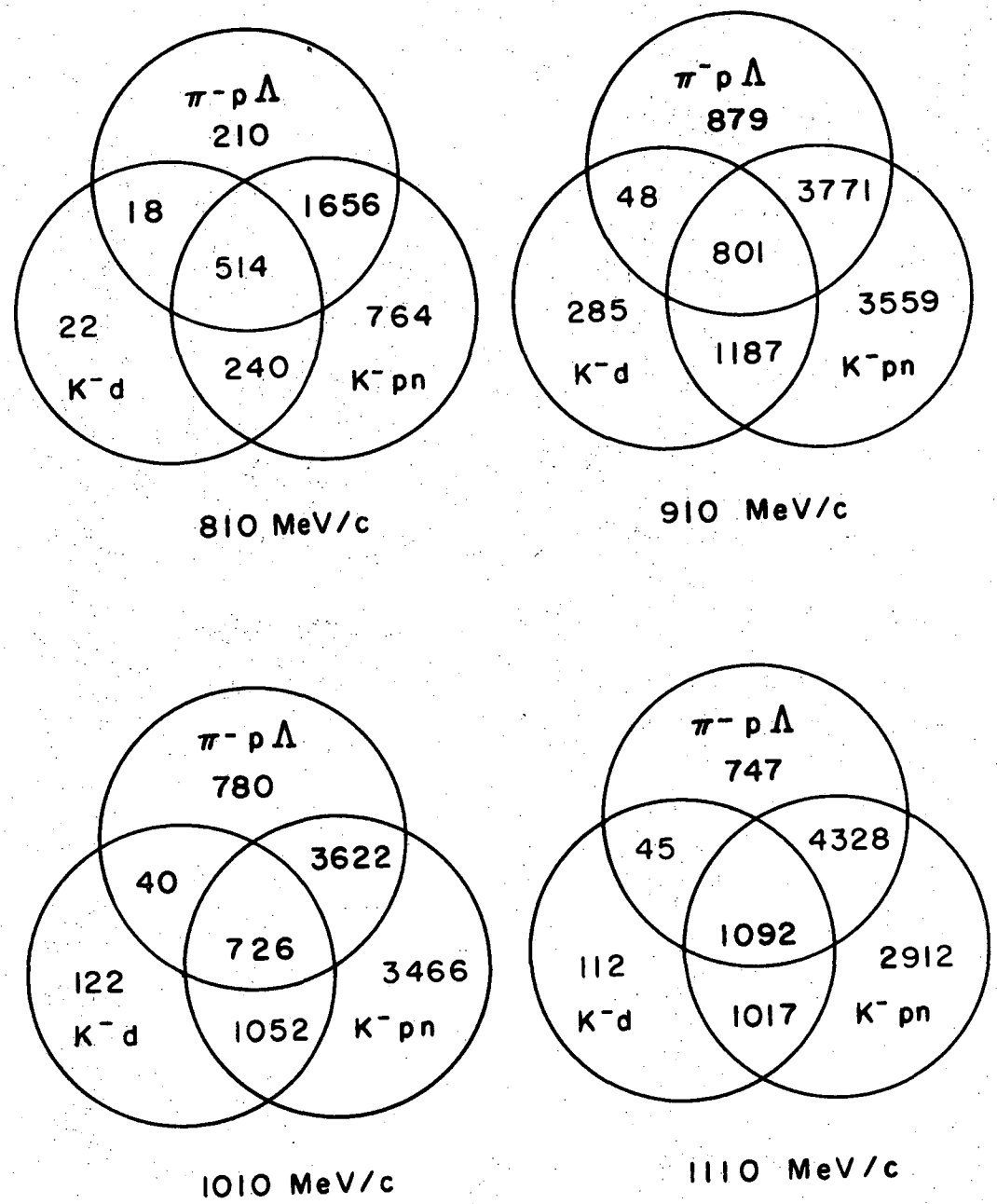

XBL703-2404

Fig. 1

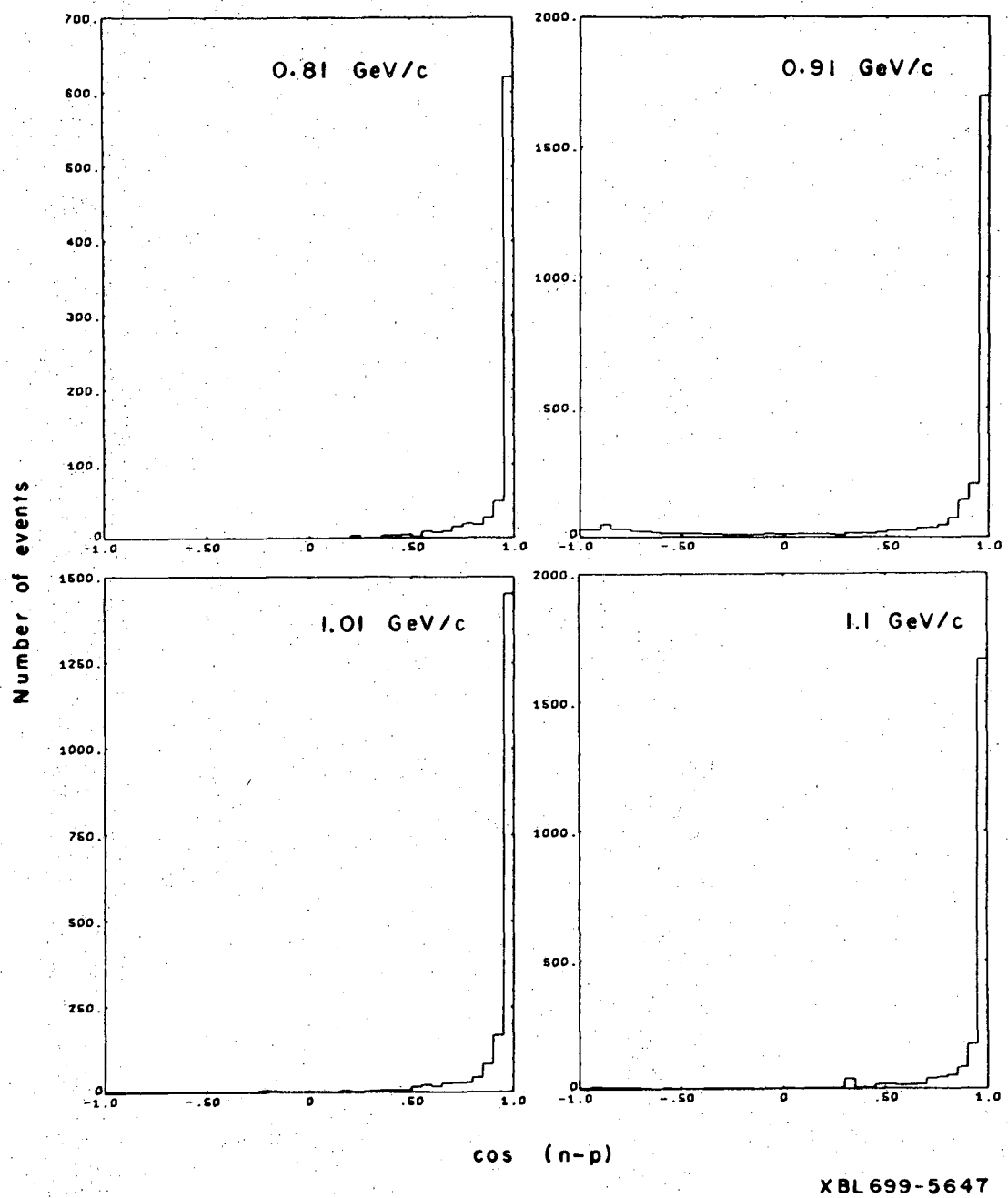
0.81 GeV/c
0.91 GeV/c
1.01 GeV/c
1.1 GeV/c
Number of events
cos (n-p)
XBL699-5647

Fig. 2

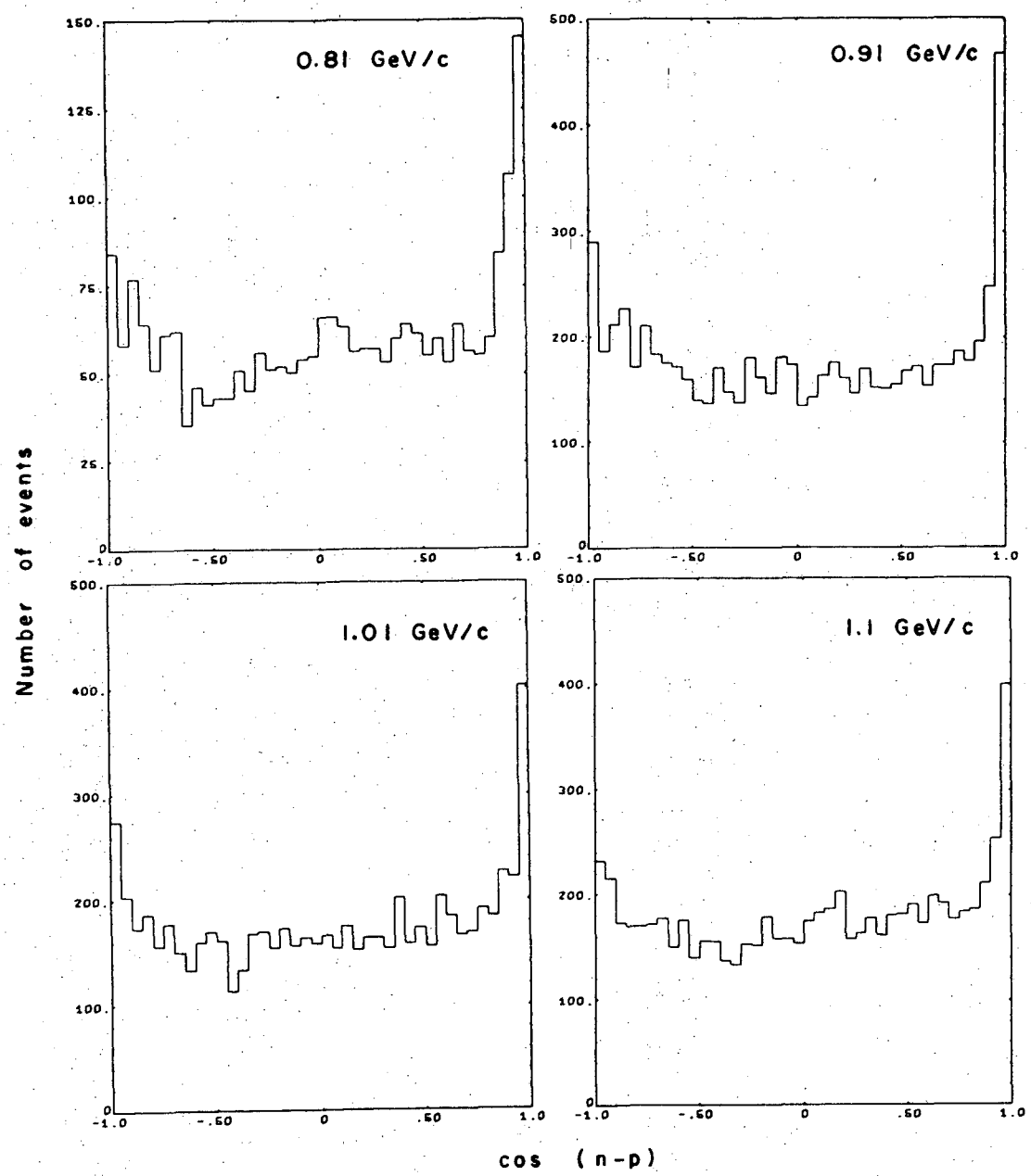

XBL 699-5660

Fig. 3

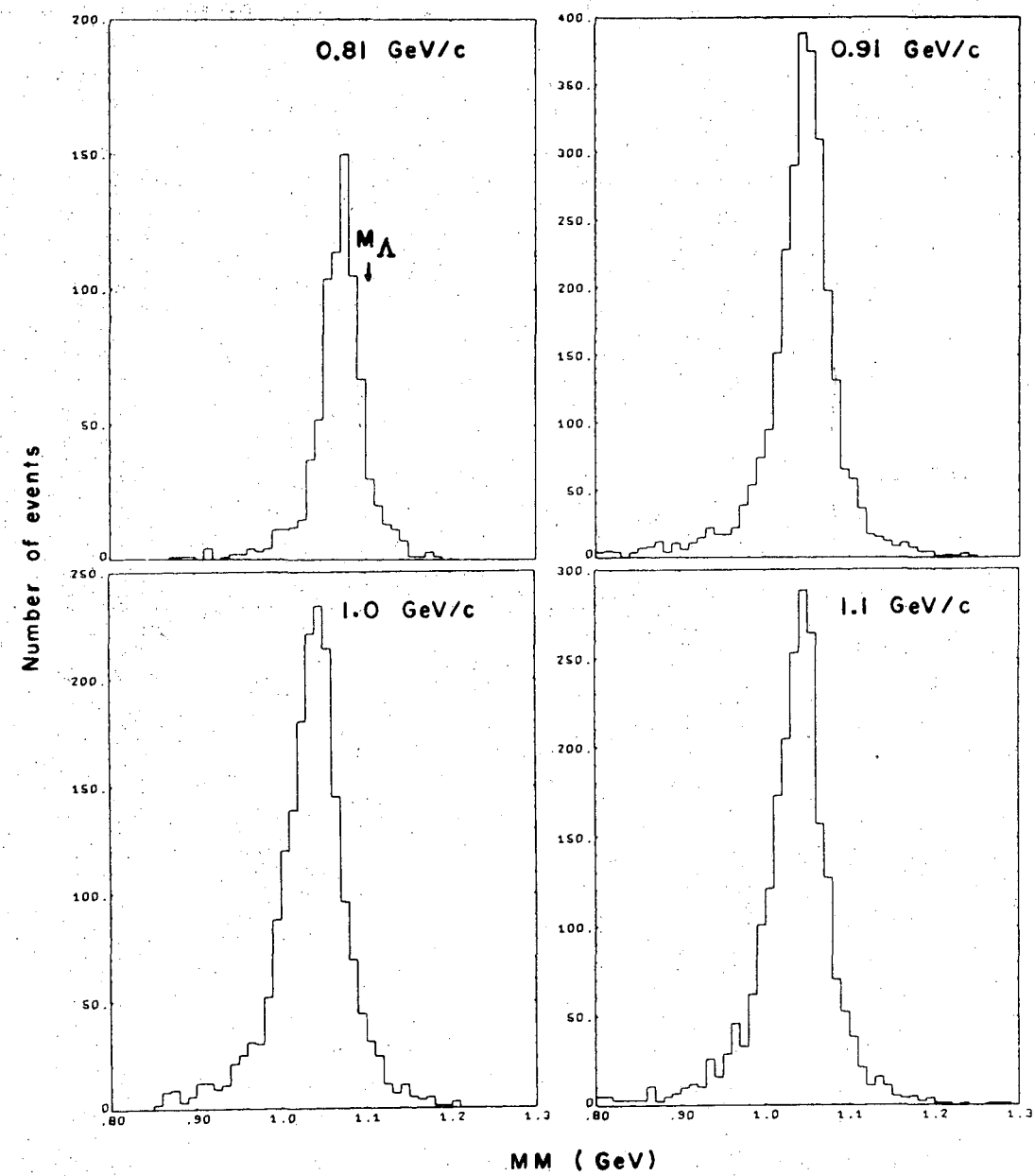

XBL 699-5650

Fig. 4

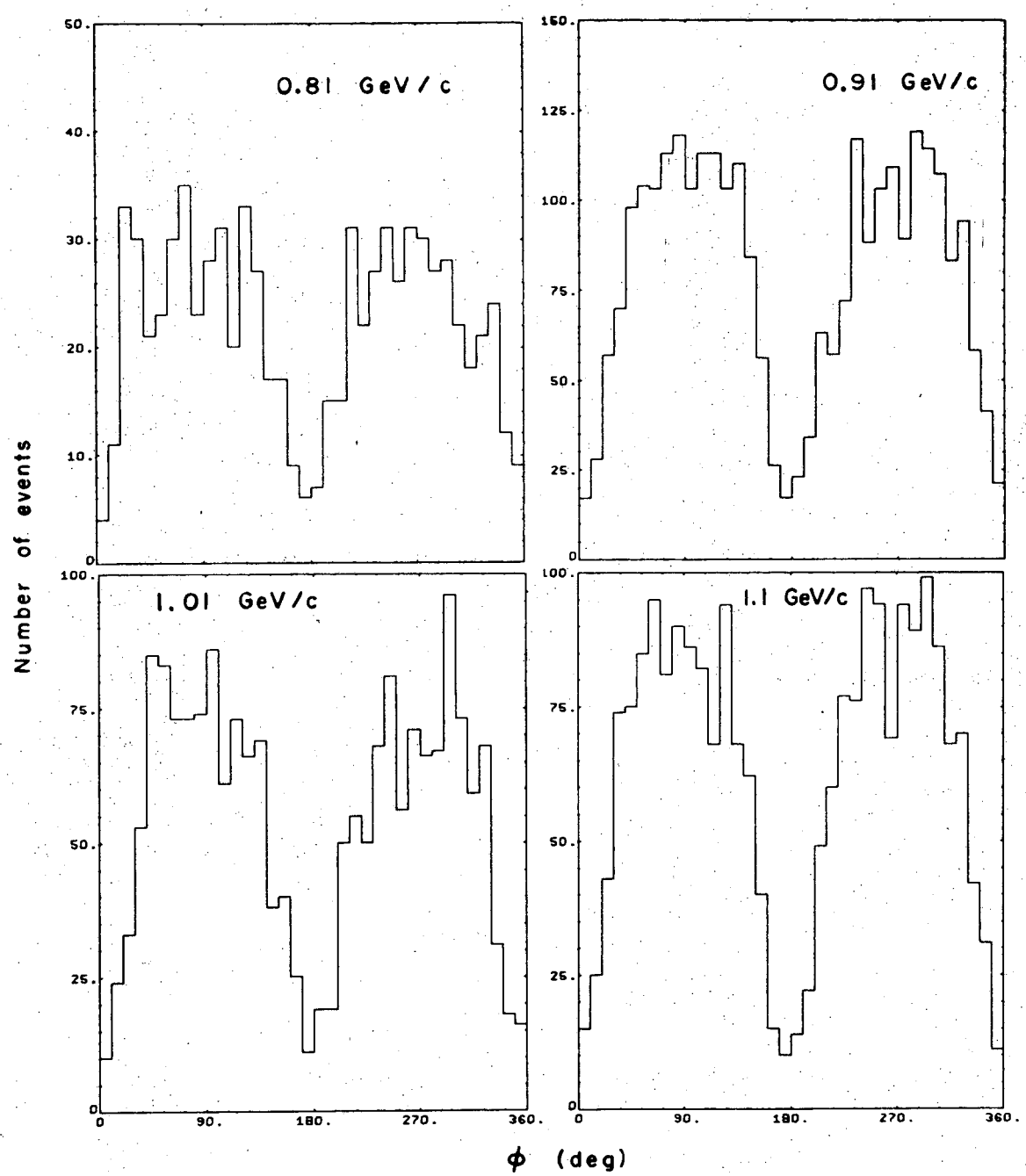

XBL 699-5653

Fig. 5

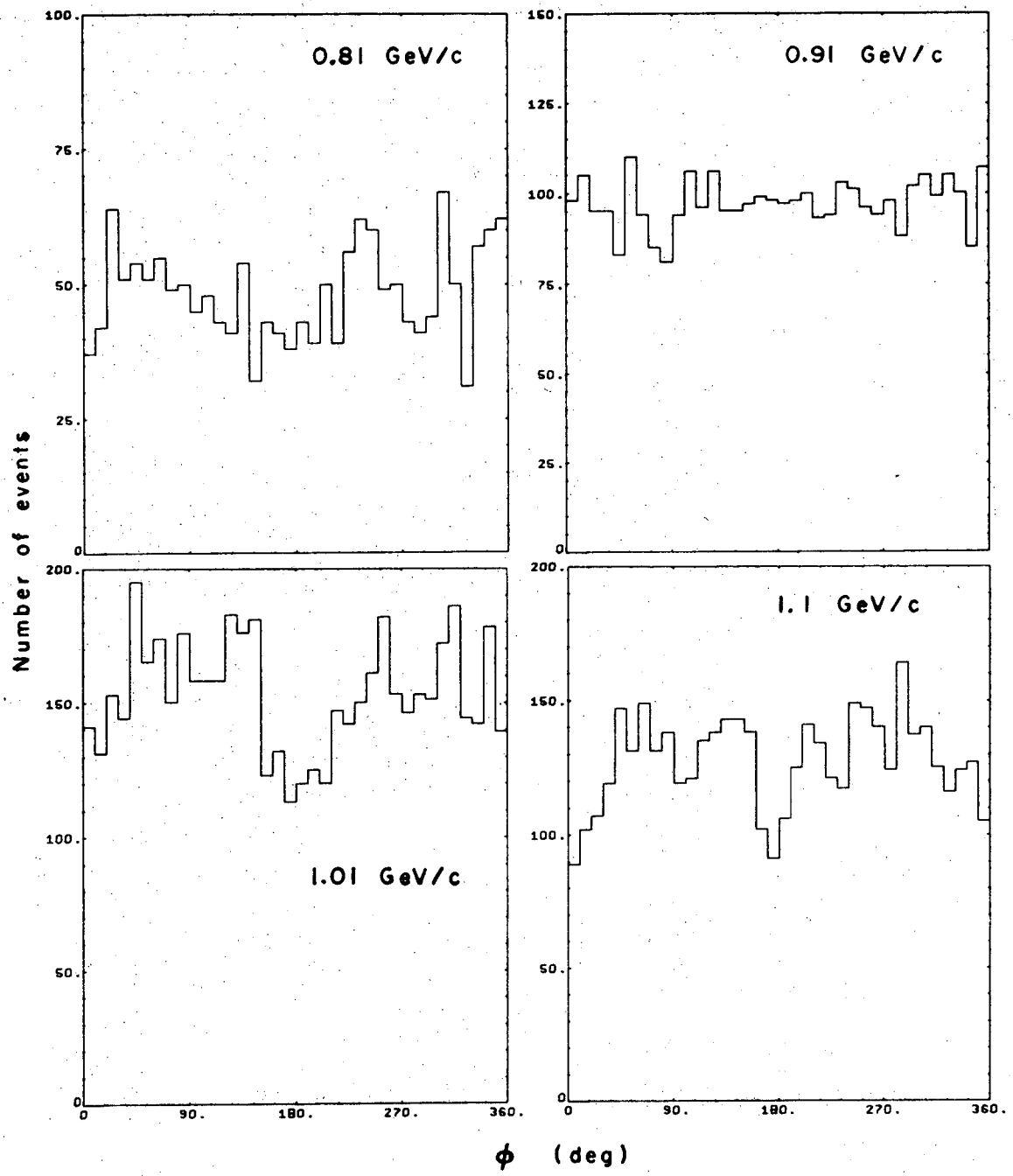

XBL 699-5651

Fig. 6

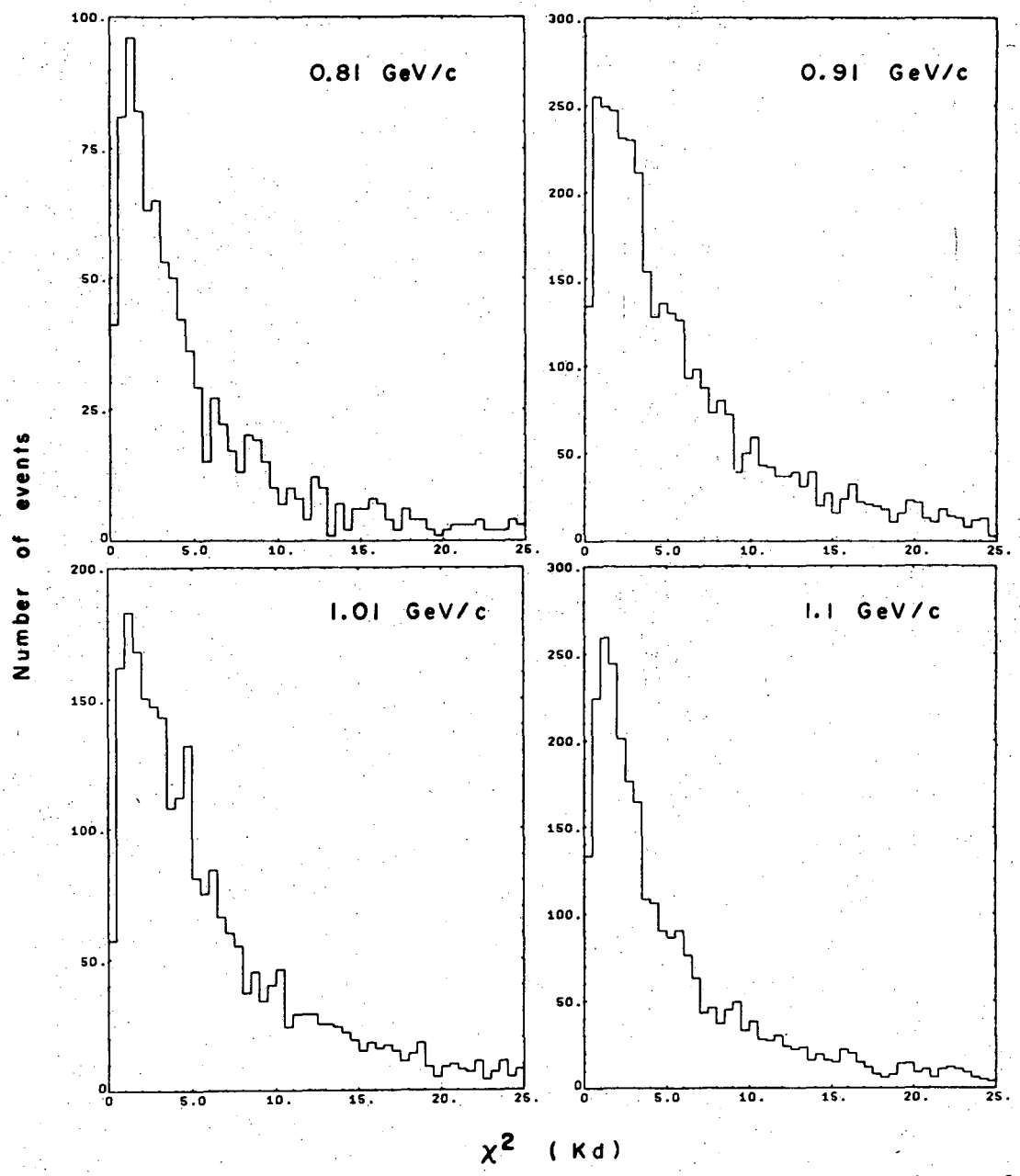

XBL 699-5652

Fig. 7

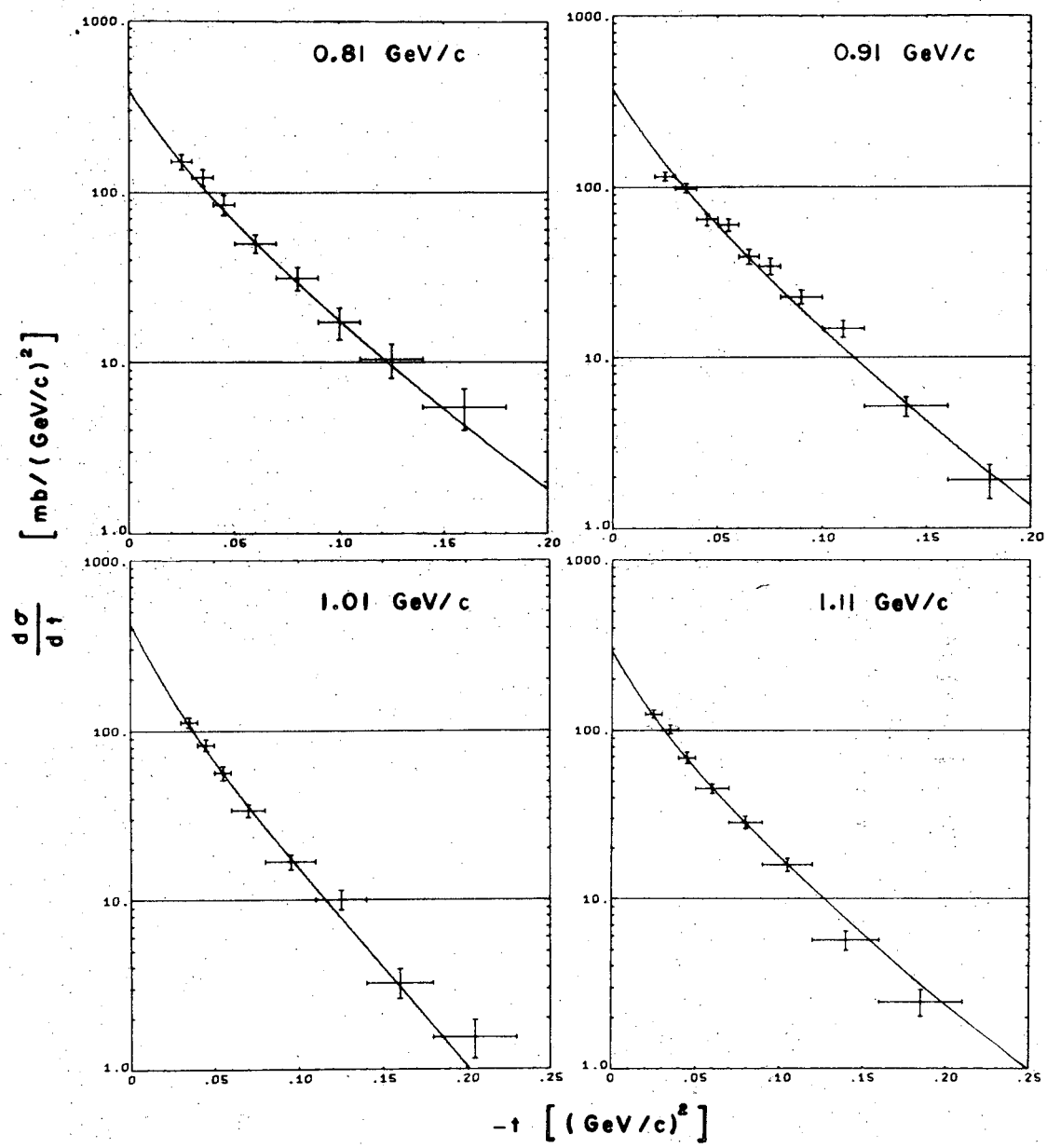

XBL 699-5659

Fig. 8

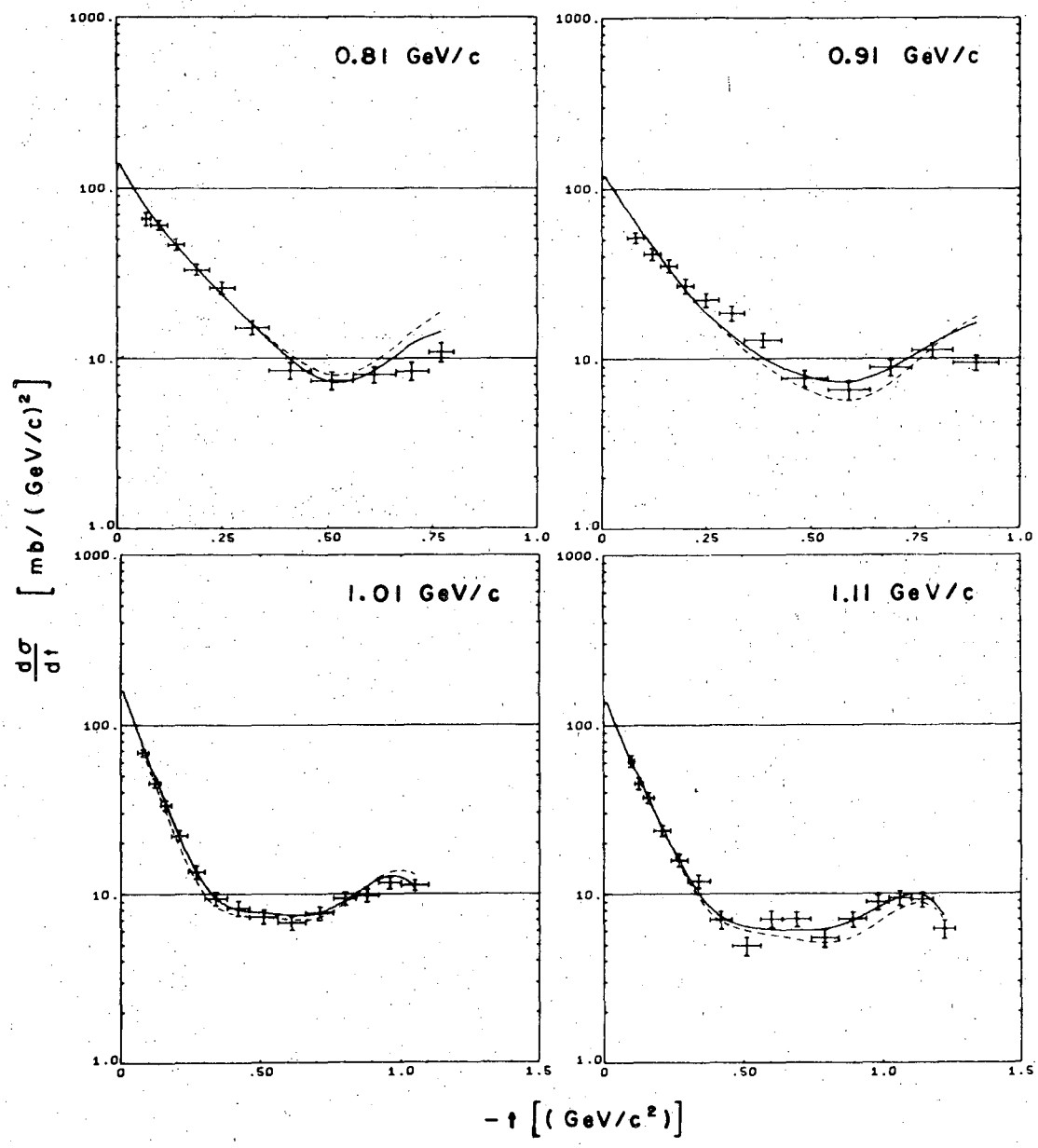

XBL 699-5688

Fig. 9

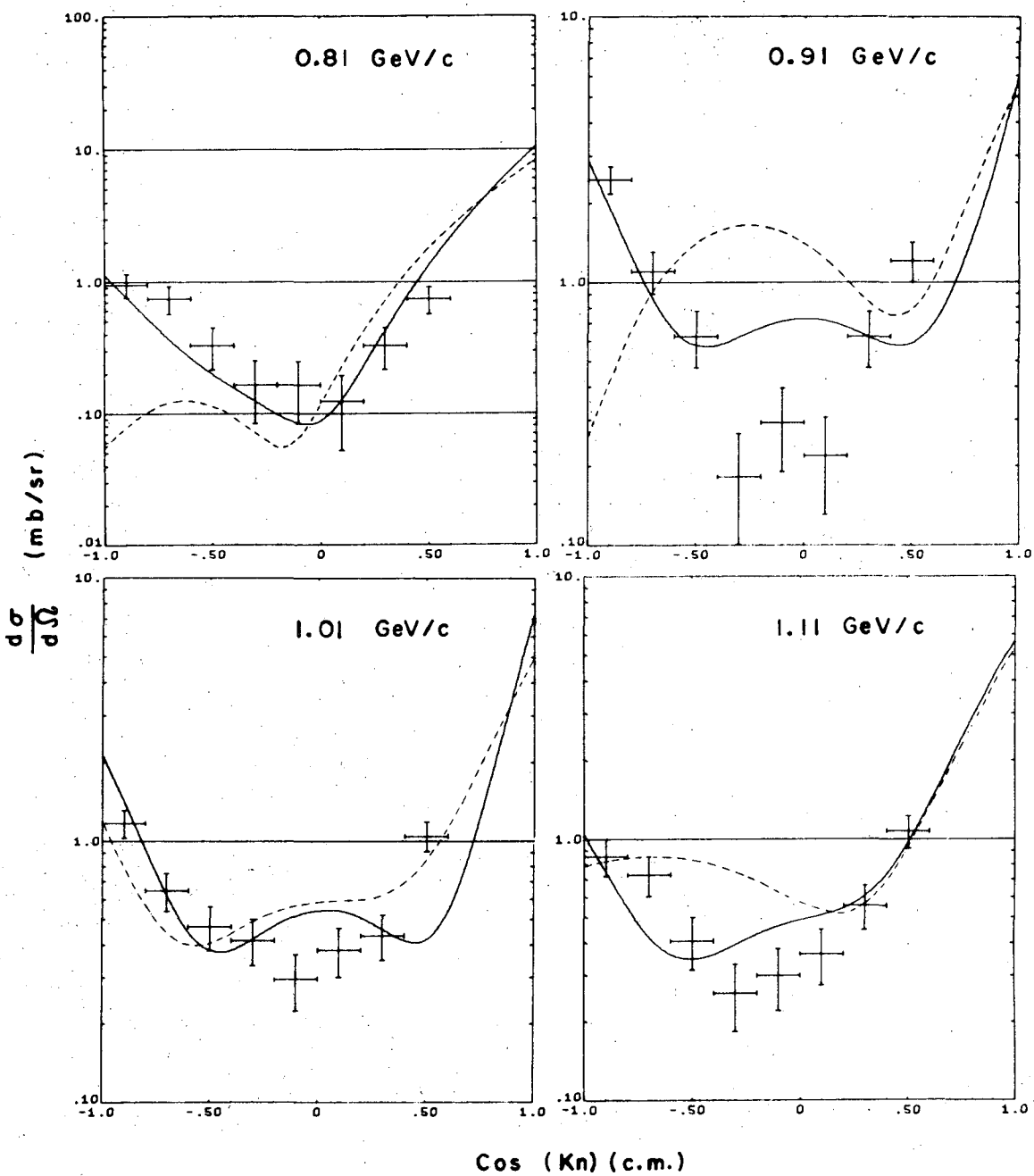

XBL 699-5686

Fig. 10

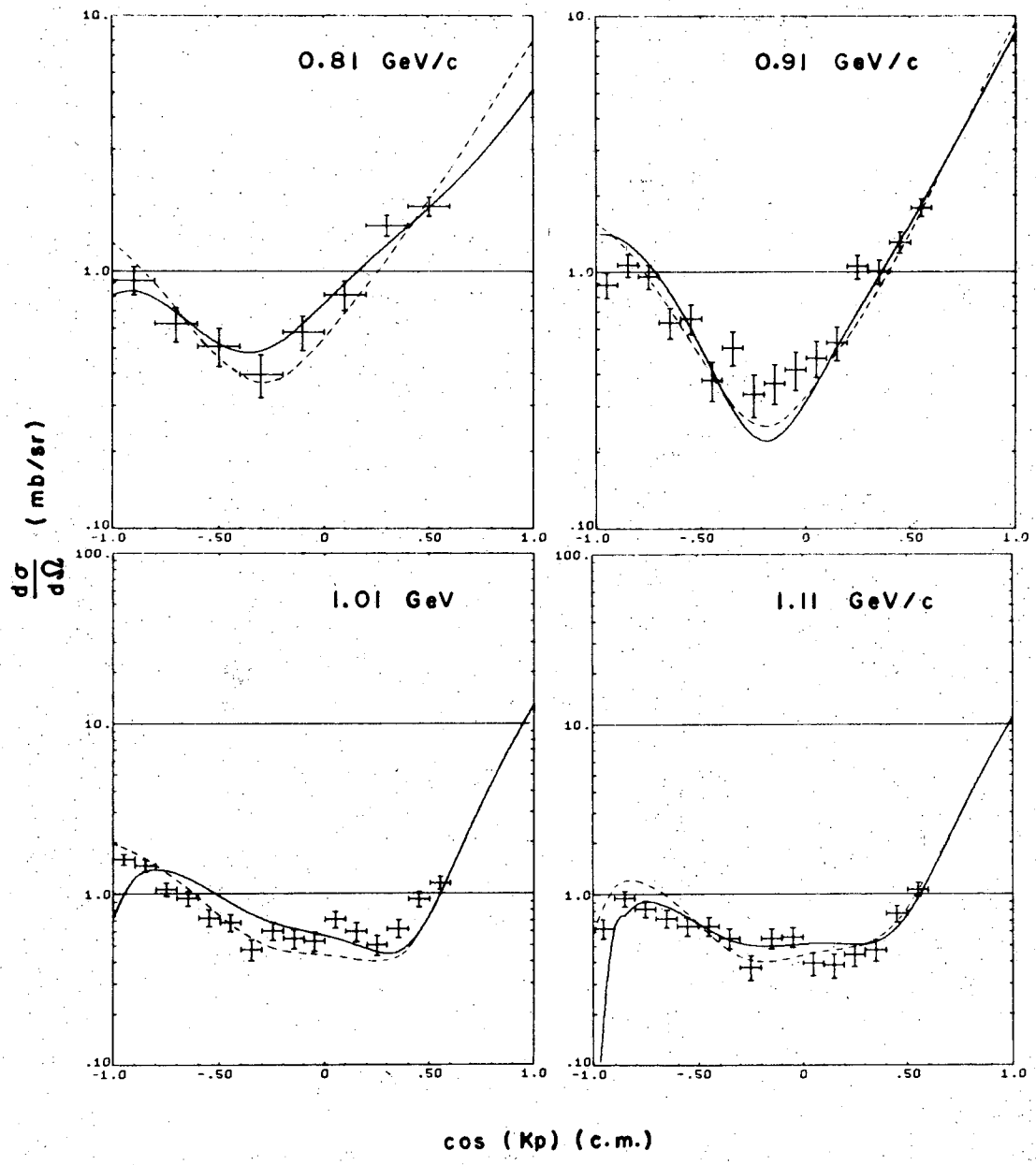

XBL 699-5685

Fig. 11

LEGAL NOTICE

This report was prepared as an account of Government sponsored work. Neither the United States, nor the Commission, nor any person acting on behalf of the Commission:

A. Makes any warranty or representation, expressed or implied, with respect to the accuracy, completeness, or usefulness of the information contained in this report, or that the use of any information, apparatus, method, or process disclosed in this report may not infringe privately owned rights; or

B. Assumes any liabilities with respect to the use of, or for damages resulting from the use of any information, apparatus, method, or process disclosed in this report.

As used in the above, "person acting on behalf of the Commission" includes any employee or contractor of the Commission, or employee of such contractor, to the extent that such employee or contractor of the Commission, or employee of such contractor prepares, disseminates, or provides access to, any information pursuant to his employment or contract with the Commission, or his employment with such contractor.

TECHNICAL INFORMATION DIVISION
LAWRENCE RADIATION LABORATORY
UNIVERSITY OF CALIFORNIA
BERKELEY, CALIFORNIA 94720